Progress in Nuclear Energy 159 (2023) 104636

Contents lists available at ScienceDirect

Progress in Nuclear Energy

journal homepage: www.elsevier.com/locate/pnucene

Analysis of radionuclide retention by the cement hydrate phase portlandite: A novel modelling approach

Oscar Almendros-Ginestà *, Tiziana Missana, Miguel García-Gutiérrez, Ursula Alonso

CIEMAT – Physical Chemistry of Actinides and Fission Products Unit, Avenida Complutense 40, 28040, Madrid, Spain

ARTICLE INFO

Keywords:
Adsorption
Radioactive isotopes
Radioactive waste
Thermodynamic calculations
Safety assessment
Engineered barriers

ABSTRACT

Cement is a widely used material for conditioning and confining radioactive waste; thus, the analysis of its sorption properties as well as of those of its main hydration products is crucial to assess radionuclide migration under disposal conditions.

In this study, the sorption of radioisotopes with different chemical properties (^{137}Cs, ^{133}Ba, ^{109}Cd, ^{152}Eu, ^{238}Pu, ^{75}Se and ^{36}Cl) in portlandite suspended in 20 mM $Ca(OH)_2$ (pH = 12.5 ± 0.2) was analyzed by means of batch sorption isotherms. In the range of the concentrations investigated, all the radionuclides showed a linear adsorption isotherm. Almost quantitative adsorption was observed for Eu, Pu and Cd, with a very high logarithm of the distribution coefficient, K_d [g·mL^{-1}] ($\log(K_d) > 5$). The adsorption of the cations Cs and Ba was significantly smaller, with a $\log(K_d)$ of approximately 2 and 0.3 respectively. The two anionic species analyzed were Cl^- and SeO_3^{2-}: whereas Cl did not show any retention, selenite showed a $\mathrm{Log}(K_d)$ of approximately 1.8. The precipitation of Se is observed for aqueous concentrations higher than $1{\cdot}10^{-4}$ M, being the precipitation of CaSeO3(s) predicted by thermodynamic calculations.

The electrokinetic surface potential of portlandite was analyzed as a function of pH (10–13.5) and with and without the presence of alkalis (0.2 M Na) to gather the basic information needed for understanding radionuclide/solid interactions and sorption modelling. The portlandite charging behaviour could be explained assuming calcium as the main ion determining the potential. This is the first time that a surface model for portlandite is proposed.

A simplified double layer modelling approach was proposed to describe experimental data, identifying the most probable sorbing species under the geochemical conditions generated by portlandite, and all the adsorption isotherms could be satisfactorily reproduced the model.

1. Introduction

Cementitious materials are envisaged in most of the designs of radioactive waste disposal facilities. The concept of Supercontainer for high-level radioactive waste consists of a carbon steel overpack surrounded by a thick concrete buffer, to decrease the income of aggressive species and decrease the overpack corrosion rate (Kursten et al., 2011). Indeed, cement is widely used for waste conditioning and containment in low and intermediate level radioactive waste disposals, being the main engineered barrier against radionuclide (RN) migration (Grambow et al., 2020).

Thus, a deep understanding of cement properties and their possible evolution is necessary to understand radionuclide retention behaviour in cementitious systems and to develop sorption models, which represent a very important tool to predict RN behaviour at a long term, and to assess the safety of radioactive waste disposals.

Dry cement, or *clinker*, is composed by several calcium silicate minerals; an ordinary Portland cement (OPC) is composed by the clinker and some gypsum (Ochs et al., 2016). Upon hydration, several phases are produced, being the calcium silicate hydrates (CSH) the most abundant forming 60–70 wt% of the cement (Duque-Redondo et al., 2021). Portlandite, $Ca(OH)_2$(s), represents about 15–25 wt% of cementitious material, being the second most abundant cement hydration phase. Portlandite forms layer type structure where the calcium atoms present an octahedral bonding structure while the oxygen atoms are tetrahedrally coordinated (Taylor, 1997).

When interacting with water, cement evolves and this interaction promotes a slow degradation process, leading to a change both in the

* Corresponding author.
E-mail address: oscar.almendros@ciemat.es (O. Almendros-Ginestà).

https://doi.org/10.1016/j.pnucene.2023.104636
Received 2 August 2022; Received in revised form 2 January 2023; Accepted 24 February 2023
Available online 7 March 2023

physicochemical properties of the solid and its equilibrium porewater. OPC, the most common cement used worldwide (Ochs et al., 2016), generates hyper alkaline conditions. This is a consequence of the hydrated cement mineral phases that act as a pH buffering solid. The degradation of cement is usually expressed in terms of pH (Taylor, 1997): a "fresh" hardened OPC cement porewater has a pH higher than 13, because of the dissolution of sodium and potassium hydroxide phases. Water progressively dilutes the alkalis, leading to a second degradation stage, Stage(II), in which portlandite is the main buffering mineral phase (Borkel, 2016). Portlandite buffers the pH around 12.5 (Atkins and Glasser, 1992; Atkinson et al., 1989; Seewald and Seyfried, 1991) and once portlandite is consumed, the system enters the third degradation stage, Stage(III), in which CSH starts dissolving and buffers pH down to 10.5 (Atkins and Glasser, 1992; Atkinson et al., 1989; Seewald and Seyfried, 1991).

Retention processes are very sensitive to the chemical conditions; therefore, they must be accounted for when mechanistic modelling is performed. Furthermore, in a heterogeneous material, it is important to understand the retention behaviour of the single mineral components, especially those dominating under certain environmental conditions.

Regarding RN adsorption processes, the main studied cement hydration products are the CSH phases, which have a very large surface area, and thus high sorption capacity for many elements (Volchek et al., 2011). Sorption models have been developed for several cationic (Ba, Cs, Ni) and anionic elements (Se) (Duque-Redondo et al., 2018; Missana et al., 2017, 2022; Ochs et al., 2016) in CSH. Nevertheless, up to date, similar studies have not been conducted with other important cement minerals as portlandite, which is especially relevant in the Stage (II) of cement degradation.

The main objective of this study is to evaluate the retention of different RNs (^{137}Cs, ^{133}Ba, ^{109}Cd, ^{152}Eu, ^{238}Pu, ^{75}Se and ^{36}Cl) in portlandite and to analyse the experimental sorption isotherms by a simplified thermodynamic modelling approach. These elements were selected for presenting different physicochemical properties: ^{137}Cs is monovalent cation with high solubility; ^{133}Ba and ^{109}Cd represent alkaline earth and transition metals, respectively. ^{238}Pu and ^{152}Eu are representative (or homologue) of actinides; ^{75}Se and ^{36}Cl are anionic species.

To establish the basis for sorption modelling, the surface potential (ζ-potential) of portlandite was measured in chemical conditions representative of Stage(I) & (II) degradation stages and as a function of pH, within the range of stability of the mineral, and its charging behaviour was described using a simplified double layer approach. This is the first time that a surface model for portlandite is developed and applied as a tool for the interpretation of RN sorption processes in cementitious environments.

Mechanistic modelling can be a very useful tool to predict the performance and safety of cement barriers and improve the *safety case,* necessary to bolster social confidence towards radioactive or nuclear waste storages.

2. Materials and methods

2.1. Portlandite synthesis and characterisation

Portlandite was obtained by recrystallization of CaO (Merck, 96% purity). The synthesis of the material has been carried out in a glove box under N_2 atmosphere to prevent carbonation of the solid. 10 g of the solid was dissolved in 1 L of purged water and stirred for 48 h. Upon the synthesis the recrystallized solid was crushed and it was suspended in 20 mM $Ca(OH)_2$(aq). This solution, in equilibrium with the solid, has an initial pH of 12.5 ± 0.1. The solid to liquid ratio used in sorption experiments was 1 or 10 g L^{-1} and, for electrokinetic experiments, 1 g L^{-1}.

The solid was analyzed by X-ray diffraction, XRD, with an Axios spectrometer from Panalytica, and attenuated total reflection Fourier transform infrared spectroscopy (ATR-FTIR) with a Nicolet iS50 equipment, with a DTGS KBr detector (resolution 4 cm^{-1}, 32 scans) on KBr-pressed discs in transmission technique in an atmosphere continuously purged from water and CO_2. FTIR analyses aim to confirm that the synthesis of the material was correct. The N_2-BET surface area of the portlandite was measured with a Micromeritics apparatus and it resulted in 13.4 ± 0.1 m^2 g^{-1}.

2.2. Sorption tests

Batch sorption experiments were carried out inside a glove box under N_2 atmosphere at a temperature of 22 ± 2 °C, suspending the solid in 20 mM $Ca(OH)_2$(aq). Sorption isotherms were carried out with the following isotopes: ^{137}Cs, ^{133}Ba, ^{109}Cd, ^{152}Eu, ^{238}Pu, ^{75}Se and ^{36}Cl, using the solutions detailed in Table 1. Pu and Se are redox sensitive elements and initially, Pu is tetravalent, and selenium is in the form of selenite. However, the oxidation state of these elements has not been checked during or after the experiments.

Sorption tests with ^{137} Cs, were carried out in the presence of 0.2 M NaCl, to evaluate the competing effects of alkali ions, in addition to the role of Ca^{2+}, the main cation present in solution.

The range of the concentration selected for each radioisotope varied according to the expected solubility under alkaline conditions. When necessary, to reach high element concentration, stable chemical were added to the radioactive isotope (as CsCl, $BaCl_2$, etc.). Upon the addition of the radionuclides, if necessary, the pH was corrected with concentrated NaOH. The final pH of the samples ranged between 12.4 and 12.6. The small changes in volume (and solid to liquid ratio) are accounted for in calculations.

Upon RN addition the portlandite suspension was maintained under rotational stirring for 7–10 days. After contact time, the solid and liquid phases were separated by centrifuging (21255 g, 30 min), with a Jouan MR23i centrifuge. This centrifugation ensures the settling of particles with a size >100 nm. Three aliquots of the separated liquid were extracted from each tube for the analysis of the final RN activity.

The activity of gamma emitters (Ba, Cd, Se, Eu and Cs) was measured with the Auto-gamma Cobra II 5003 (Packard) with 3″ detector of NaI (TP). The activity of alpha-beta emitters (Pu, Cl) was measured with a liquid scintillation analyser Tri-Carb 4910 TR (PerkinElmer) and using Ultima Gold™ as a scintillation cocktail. The uncertainty for the counting procedure (for both gamma and alpha-beta measurements) is less than 2%.

Table 1 summarizes the details of the experimental conditions used for the sorption isotherms.

The distribution coefficient (K_d), was obtained to quantify the extent of RNs adsorption and it is defined as:

$$K_d = \frac{[RN]solid}{[RN]eq} \cdot \frac{V}{m} \quad \text{E.1}$$

$[RN]_{eq}$ represents the radionuclide activity [Bq·mL^{-1}] that remained in the aqueous phase at the equilibrium; $[RN]_{solid}$ is the concentration adsorbed in the solid given by the difference between the initial and final activities (($[RN]_{in}$ - $[RN]_{eq}$) [Bq·mL^{-1}]); V is the volume of the solution [mL] and m the mass of the solid [g].

Table 1
Details of the initial conditions of sorption isotherms. pH = 12.4–12.6; Ca = 20 mM. Solid to liquid ratio 1–10 g L^{-1}.

Radioisotope	Radionuclide Solutions	Concentration Range (M)
^{75}Se	H_2SeO_3 in 0.1 M HCl	[10^{-11} - 10^{-3}]
^{133}Ba	$BaCl_2$ in 0.1 M HCl	[10^{-8} - 10^{-4}]
^{109}Cd	$CdCl_2$ in 0.1 M HCl	[$2{\cdot}10^{-8}$ - 10^{-3}]
^{137}Cs	CsCl in 0.1 M HCl	[10^{-8} - 10^{-4}]
^{238}Pu	$Pu(NO_3)_4$ in 4 M HNO_3	[$7{\cdot}10^{-11}$ - $9{\cdot}10^{-9}$]
^{152}Eu	$EuCl_3$ in 0.1 M HCl	[$7{\cdot}10^{-10}$ - 10^{-4}]
^{36}Cl	NaCl in deionized water	[$2{\cdot}10^{-6}$ - 10^{-2}]

2.3. Zeta potential measurements

The surface potential (ζ-potential) of the portlandite was measured by Laser Doppler electrophoresis, with a Malvern Zetamaster apparatus equipped with a He–Ne laser (λ = 633 nm). The surface potential was analyzed on suspensions prepared at a concentration of 1 g/L in $Ca(OH)_2$ 20 mM, varying pH from 10 to 13, which is the range of portlandite stability. The equilibrium pH of the suspension was 12.5; the changes of pH were obtained by adding aliquots of concentrated NaOH or HCl.

To analyse the possible effect on the surface potential of the ionic strength and the presence of alkalis, which are abundant in the cement porewater during Stage (I), electrophoretic measurements as a function of pH were also carried out in the presence of 0.2 M NaCl. Additionally, the portlandite ζ-potential was measured in two synthetic waters representative of Stage (I) and Stage (II) of cement degradation. The composition of these waters is given in Table 2.

Upon the zeta potential measurement, some samples were centrifuged (9000 g, 30 min) and the supernatant analyzed to measure the Ca concentration and to determine the degree of dissolution/precipitation of portlandite during the test.

2.4. Modelling

As to maintain the modelling approach as simple as possible, portlandite was considered as a simple oxide, with a generic amphoteric surface site "SOH", which density is considered to be 2.31 sites/nm^2 (3.84 μmol/m^2), a value suggested for many natural oxides (Payne et al., 2013).

In a generic oxide, SOH sites can be protonated or deprotonated depending on pH, but considering the pH of interest for portlandite (pH > 10), only the deprotonation reaction will be significant:

$$S-OH \underset{K}{\rightarrow} 1S-O^- + H^+ \qquad \text{E.2}$$

Considering a double layer model approximation, the intrinsic equilibrium constant of this reaction is K_1, being the mass law equation corresponding to the reaction E.2:

$$K_1 = \frac{(SiO^-)\{H^+\}}{(SiOH)} exp\left(-\frac{F\Psi_d}{RT}\right) \qquad \text{E.2a}$$

Where {} represent the ion activity and (#) ion concentration. Ψ_d is the diffuse potential, R the molar gas constant, T the absolute temperature and F the Faraday constant. The coulombic term accounts for the electrostatic effects.

In general, the adsorption of cations (M^{z+}) on these sites will be determined by equilibrium reactions as:

$$S-O^- + M^{z+} \underset{K_M}{\rightarrow} S-OM^{(z-1)+} \qquad \text{E.3}$$

Proposed surface reactions are described in results section.

The calculations needed for the modelling of the surface charge of portlandite (ζ-potential) and of the sorption isotherms were carried out using the geochemical software CHESS (Chemical Equilibrium of Species and Surfaces, v2.4) which is used in many scientific areas, notably in environmental engineering, safety and performance assessment of waste repositories and ground- and surface water pollution studies (Van der Lee and de Windt, 1999).

The thermodynamic database used for RNs speciation and sorption calculations is the Andra's (French National Radioactive Waste Management Agency) ThermoChimie database (TCDB) version 10 d (Begg et al., 2021), because this is one of the most complete and up to date database, for elements of interest for radioactive waste management available nowadays and based on the OECD-NEA TDB project (Östhols and Wanner, 2000).

3. Results

3.1. Portlandite characterisation

Fig. 1a shows the FTIR-ATR spectrum of the synthetized portlandite material compared to the theoretical spectra of calcium hydroxide, and Fig. 1b the XRD diffractogram.

The FTIR-ATR spectra (Fig. 1a), presents the characteristic peak of 3640 cm^{-1} which corresponds to the stretching of O–H bound present in portlandite while the other peaks are related to Ca–O lattice vibrations (Chollet and Horgnies, 2011; Fernandez-Carrasco et al., 2012; Horgnies et al., 2013).

The XRD diffractogram confirms that the solid is portlandite. In some analyses, peaks attributed to traces of calcite were found, probably due to the carbonation of the sample when taken out samples from the anoxic glove box for characterisation.

3.2. RN sorption isotherms

Fig. 2 shows the adsorption isotherms of the analyzed radionuclides represented as the logarithm of the distribution coefficient (K_d) *vs* the logarithm of the equilibrium concentration in solution. Fig. 2a shows the sorption isotherms of ^{152}Eu and ^{238}Pu; Fig. 2b the isotherms of ^{109}Cd, ^{137}Cs (performed adding NaCl 0.2 M to the suspension) and ^{133}Ba and Fig. 2c the isotherm of ^{75}Se.

The highest sorption values ($Log(K_d) > 5$) were observed for Cd, Eu and Pu. Due to the very high retention, Eu and Pu data presents the largest experimental dispersion. Furthermore, while Pu for S/L ratio of 10 g/L shows linear sorption, for 1 g/L a clear drop on sorption is observed as the Pu concentration increases. This could be attributed to the possible formation of colloids, which cannot be separated by centrifugation.

Elements like Cs and Ba, that in natural materials are usually retained by cationic exchange, show much less adsorption with a Log (K_d) ≈2 for Cs and Log(K_d) ≈0.3 for Ba. Selenite, which is an anionic aqueous species, is retained by portlandite with a mean Log(K_d) ≈1.8. Sorption isotherm of ^{36}Cl was carried out for the concentration range of $1{\cdot}10^{-6}$ up to $1{\cdot}10^{-2}$ M, but retention was always under the detection limit, thus data are not included in the Figure.

Within the range of analyzed concentrations, all the RN sorption isotherms in portlandite showed linear behaviour. Only in the case of selenium, a sudden increase of K_d values is detected in the sorption isotherms when increasing the initial RN concentration. This behaviour is generally attributed to the element precipitation.

3.3. Portlandite's surface potential

The ζ-potential values measured for the portlandite suspended in the waters representative of Stage (I) and Stage(II) are plotted in Fig. 3, as an orange diamond and a red square, respectively. Under the Stage(I) porewater conditions (pH = 13.4 and [Na] = 1900 mg/L), the zeta potential is negative (−20 mV), whereas under Stage(II) conditions (pH = 12.6 and [Na] = 80 mg/L) the potential is positive (17 mV).

Table 2
pH and composition of cement water for stage I and II. Elemental concentration in mol/L. Errors in concentrations are <5%.

Degradation Stage	pH (±0.1)	$[Na^+]$	$[K^+]$	$[Ca^{2+}]$	$[SO_4^{2-}]$	$[Cl^-]$	$[SiO_2]$
Stage I (fresh)	13.4	$8.26{\cdot}10^{-2}$	$1.83{\cdot}10^{-1}$	$5.5{\cdot}10^{-4}$	$1.28{\cdot}10^{-3}$	$1.95{\cdot}10^{-4}$	$4.49{\cdot}10^{-5}$
Stage II (degraded)	12.6	$3.48{\cdot}10^{-3}$	$6.15{\cdot}10^{-3}$	$8.50{\cdot}10^{-3}$	$1.04{\cdot}10^{-5}$	$6.49{\cdot}10^{-4}$	$8.16{\cdot}10^{-6}$

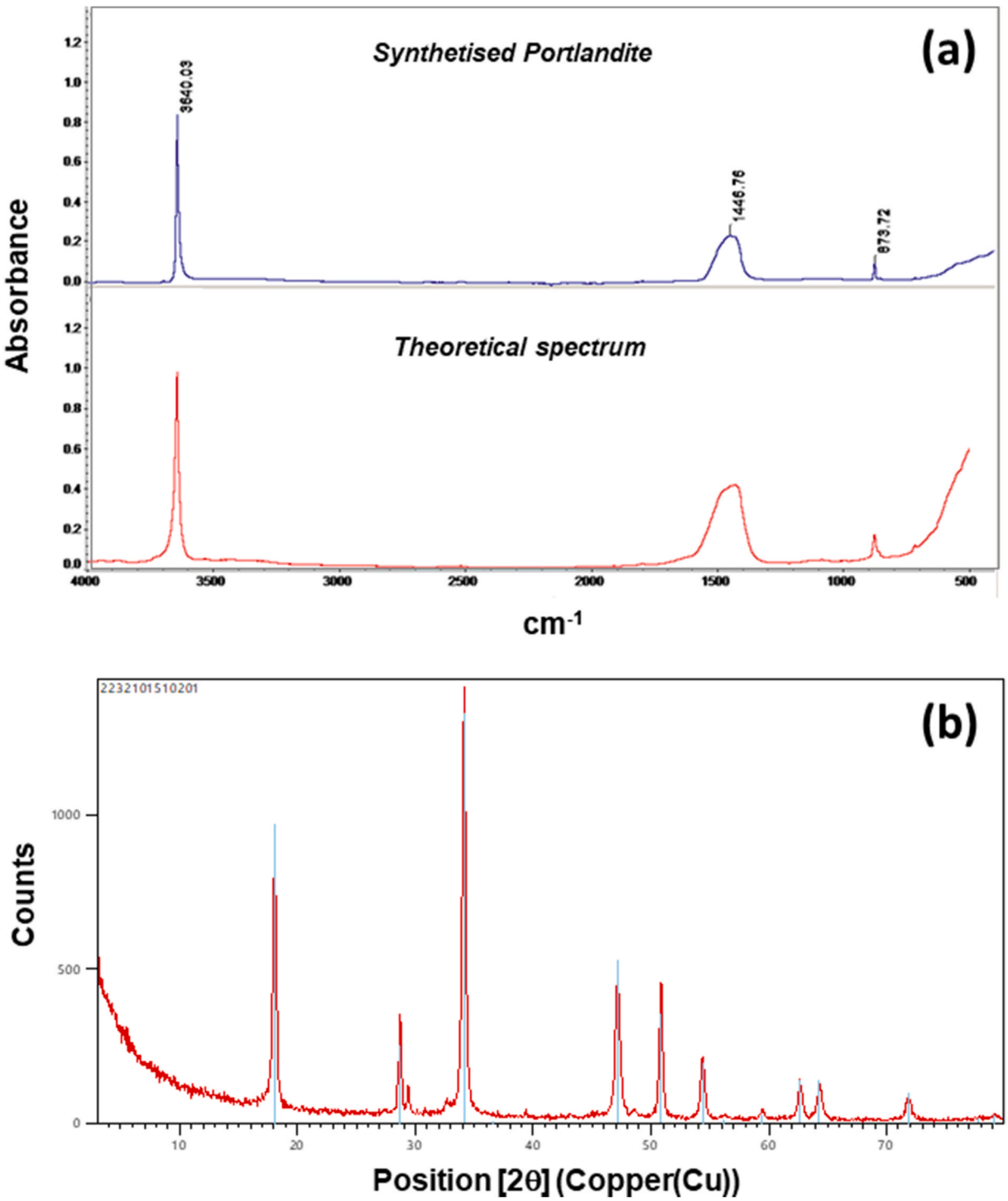

Fig. 1. a) FTIR-ATR and b) XRD spectra of the portlandite synthetized in laboratory and theoretical calcium hydroxide and portlandite spectra.

To better elucidate the surface charge evolution of portlandite, the dependence on pH of the ζ-potential of portlandite in its equilibrium water (20 mM $Ca(OH)_2$ (aq)), in the presence of [Na] = 0.2 M and absence of alkalis, was analyzed and the results are summarized in Fig. 3.

From pH 10 to 12.5, in both systems ($Ca(OH)_2$ (aq) with and without NaCl), the potential is positive and stable, within the experimental error. However, at higher pH, the magnitude of the ζ-potential suffered a decrease of approximately 15 mV. For pH around 13, the portlandite ζ-potential drops sharply to zero in both cases.

In the literature, specific studies for understanding the surface charge properties of portlandite for adsorption modelling purposes could not be found; however (Timmons et al., 2020), studying the theological and dispersion behaviour of portlandite, reported an isoelectric point around pH 13, in agreement with our experimental data.

Both the addition of NaCl and pH changes can modify portlandite environment. The samples of portlandite with added NaCl, used for the measurement of the ζ-potential, were centrifuged to quantify the Ca concentration in the supernatant to gather information on dissolution/precipitation processes of portlandite as the pH varies. The results are summarized in Table 3.

Results showed that the quantity of aqueous Ca is approximately

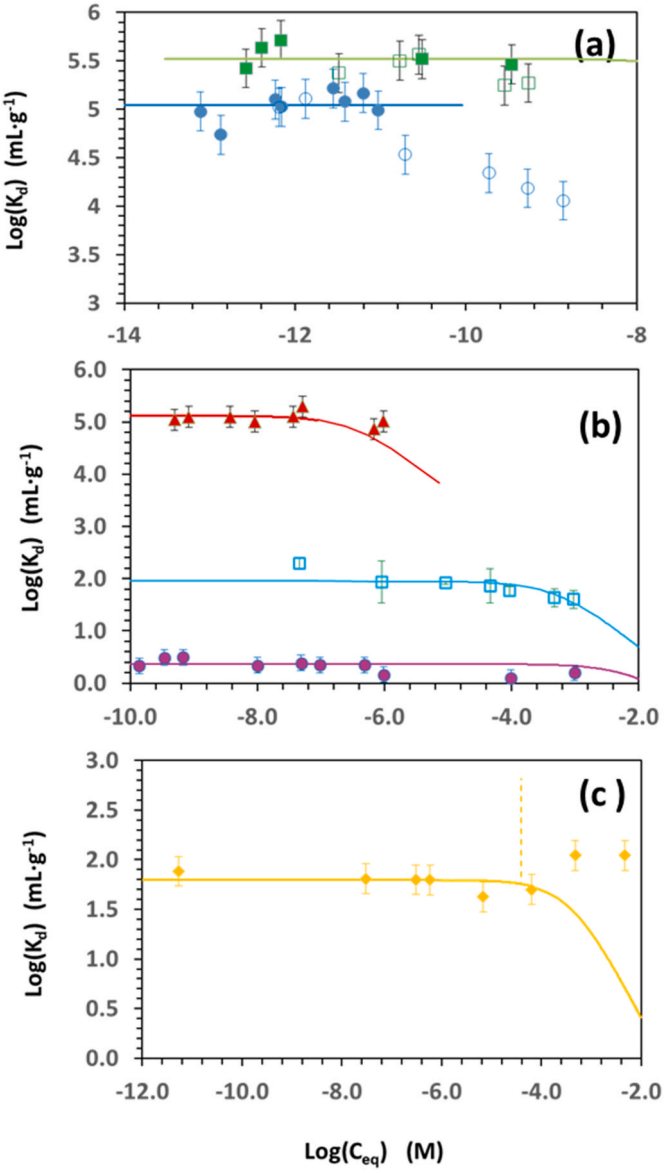

Fig. 2. Sorption isotherms in portlandite for a) ^{152}Eu (square) and ^{238}Pu (circle); b) ^{109}Cd (triangle); ^{137}Cs (square); ^{233}Ba(circle) and c) ^{75}Se (diamond). Open points correspond to a 1 g L^{-1} of portlandite, solid points to 10 g L^{-1} pH 12.5 ± 0.2. Continuous lines correspond to model calculations with the parameters of Table 4. Dashed line, in Fig. 2b, corresponds to the theoretical adsorption isotherm of Cs in the absence of Na, also calculated with the parameters of Table 4.

constant from pH 10.5 to pH 12, then it decreases significantly. The loss of aqueous Ca for pH higher than 12.5, means that further solid is precipitating causing an increase of the portlandite in the system, which must be accounted for. The decrease of Ca additionally produces a decrease in the ζ-potential, showing that Ca is the main responsible of the charging behaviour of the portlandite, thus it can be considered as the ion determining the potential (IDP). In any case, it has been shown that Ca consumption is not only determined by adsorption/desorption processes, but also by the precipitation of the solid itself that must be considered in modelling calculations.

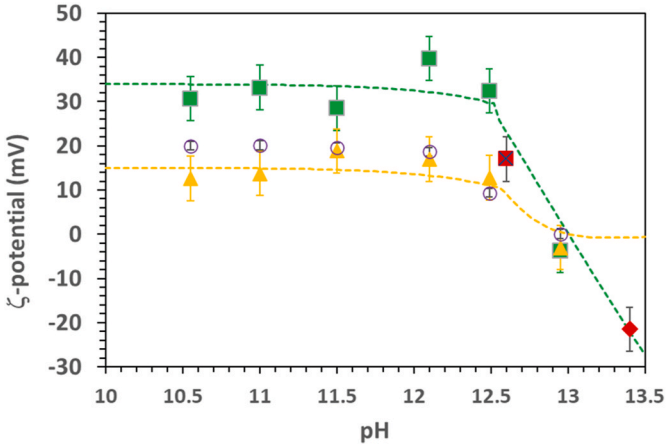

Fig. 3. ζ-potential of portlandite as a function of pH in 20 mM $Ca(OH)_2$(aq) (▲) with and (■) without NaCl 0.2 M. The potential of the portlandite measured in Stage(I) and Stage(II) cement waters are represented by the red diamond and square respectively. The purple circles (○) represent the point-to-point calculations performed pH and [Ca] concentration values of Table 2. Dotted lines correspond to model calculations with the parameters of Table 3.

Table 3
Experimental measurements of aqueous Ca, as a function of pH in the presence of portlandite and 0.2 M NaCl.

pH	[Ca] ($mg{\cdot}L^{-1}$)	ζ-potential (mV) Experimental	ζ-potential (mV) Calculated point-to-point (±3 mV)[a]
10.5	1080	12.6 ± 0.75	20.0
11.0	1100	13.7 ± 3.34	20.1
11.5	1090	18.8 ± 1.48	19.6
12.0	1100	17.0 ± 1.04	18.7
12.5	580	12.8 ± 3.07	9.4
13.0	200	−3.0 ± 1.46	0.05

[a] These values are calculated with the CHESS code.

4. Modelling and discussion

4.1. Portlandite surface charge

As first step to develop the double layer sorption model, the surface electrostatic charge behaviour exhibited by portlandite was analyzed. Considering the zeta potential experimental data of Fig. 3, we need to reproduce the charge evolution of the portlandite in its equilibrium water, as a function of pH, also in the presence of Na, and including the variation of Ca concentration in the system due to precipitation/dissolution processes (Table 3).

In Fig. 3 and Table 3, it could be observed that portlandite ζ-potential depends on the presence of Ca in solution which, on turn, depends on the precipitation (and dissolution) of the solid. As the ζ-potential of the solid is positive, when Ca concentration is stable in solution, we can assume that the portlandite surface charge is determined by the adsorption of Ca in the deprotonated S–OH site according to this equation:

$$S-O^- + Ca^{2+} \underset{K_{Ca}}{\rightarrow} S-OCa^+ \qquad \text{E.4}$$

In the presence of NaCl, the surface charge of portlandite decreases and this effect can be attributed to the adsorption of Na which competes with Ca, and forms neutrally charged surface specie (E.3).

To determine the constants of the main reactions E.1 – E.2, E.4, and the complexation constant for Na (E.3), we assumed that the diffuse potential (Ψ_d) of the double layer model, can be represented by the experimental ζ-potential (Missana et al., 2017).

In the model, portlandite is described as a generic solid with SOH surface sites groups where sorption processes occur and to maintain the

Table 4
Surface reactions and parameters used to fit the ζ-potential behaviour of portlandite. The logK is referred to the description of the surface complex in the code. The maximum error for the LogK, considering the experimental data is ±0.2.

Reaction	Species description in the CHESS Code	LogK
$SOH \Leftrightarrow SO^- + H^+$	SO^- = 1 SOH, −1 H^+	−6.8 ± 0.2
$SO^- + Ca^{2+} \Leftrightarrow SO–Ca^+$	$SO–Ca^+$ = 1 SOH, −1 H^+, 1 Ca^{2+}	−3.6 ± 0.2
$SO^- + Na^+ \Leftrightarrow SO–Na$	SO–Na = 1 SOH, −1 H^+, 1 Na^+	−4.0 ± 0.2
BET = 13.4 ± 0.1 m^2/g Site density = 3.84 μmol/m^2		

chemical equilibrium of the system in the calculations, dissolution/precipitation processes were allowed.

The experimental curves are fit stepwise according to a trial-and-error procedure. The curve without Na has been simulated first, and the LogK of the reaction $SO^- + Ca^{2+} \Leftrightarrow SO–Ca^+$, has been adjusted until the calculated zetapotential, reached the mean experimental zetapotential (observed between pH 10.5 and 12.5). Then the obtained valued was fixed, and the process was repeated with the data in the presence of Na, to determine the log K of the reaction $SO^- + Na^+ \Leftrightarrow SO–Na$.

The mean equilibrium constant for deprotonated SOH sites and the complexation constants obtained for Na^+ and Ca^{2+} needed to simulate the experimental data are summarized in Table 4.

The estimated ζ-potentials for portlandite with and without NaCl 0.2 M are superimposed to the experimental data in Fig. 3 as a dotted line. The selected model reproduces quite satisfactorily the experimental data.

To reinforce these results, the ζ-potential calculations were performed point-to-point using the pH and Ca concentrations reported in Table 3, and recalculating concentration of portlandite, when further precipitation occurs. The results obtained are plotted as open circles in Fig. 3, and these calculations fitted also quite well the experimental data.

Considering the pH, Na and Ca content of the fresh and Stage(II) degraded water, the ζ-potential calculated were −5.6 and + 18.7, respectively. The potential is underestimated in the case of the fresh water, where possibly the effects of other ions at high concentration (for example potassium or sulphate) should be also accounted for.

Once the parameters defining the surface of the portlandite were determined (Table 4) it was possible to propose complexation reactions with the portlandite S–OH surface sites for all the studied RNs.

4.2. RN sorption modelling

To determine the possible surface complexes, the speciation of all the radionuclides was calculated, considering the chemical conditions generated by portlandite ([Ca] = 20 mM and pH 12.5). For the speciation calculations, the RN concentration was set to $1{\cdot}10^{-8}$ M. Table 5 shows the results of the speciation calculations, for each radionuclide the mayor aqueous species is indicated. Under experimental conditions, speciation calculations predicted radionuclide precipitation. However, experimentally obtained sorption isotherms only suggest precipitation in the case of selenium (Fig. 2). Therefore, RN precipitation was excluded in further simulations.

A standard double layer model was considered to model adsorption isotherms, assuming that only charged aqueous species can interact with the surface functional groups of portlandite.

If the aqueous species is positively charged, surface complexation on portlandite will occur directly on the deprotonated site, SO^-, (E.2).

If the aqueous species is negatively charged, we assume that the complexation can occur through the bridge with Ca (E.4) in a reaction of this type:

Table 5
Species, complexes, and parameter used to fit K_d values in the sorption isotherms. Solids are excluded from calculations if precipitation is not experimentally seen. The logK is referred to the description of the surface complex in the CHESS code.

Mayor aqueous species	Species used for complexation	Mean Kd (mL/g)	Complex// Reaction description	LogK (±0.2)
Ca[2+]	Ca[2+]	1.3 (calculated)	SOCa[+] = 1 SOH, −1 H[+], 1 Ca[2+]	−3.61
$Eu(OH)_3$ (>99%)	$Eu(OH)_2$[+] (1.2%)	$4.6{\cdot}10^5$	SOEu$(OH)_2$ = 1 SOH, −3 H[+], 1 Eu[3+], 2 H_2O	−12.85
$Pu(OH)_4$ (>99%)	$Pu(OH)_3$[+] (<1%)	$1.3{\cdot}10^5$	SOPu$(OH)_3$ = 1 SOH, −4 H[+], 1 Pu[4+], 3 H_2O	+4.35
$Cd(OH)_3$[-] (59%)	$Cd(OH)_3$[-]	$1.3{\cdot}10^5$	SOCaCd$(OH)_3$ = 1 SOH, −4 H[+], 1 Ca[2+], 1 Cd[2+], 3 H_2O	−30.40
Ba[2+] (94%)	Ba[2+]	2.3	SOBa[+] = 1 SOH, −1 H[+], 1 Ba[2+]	−3.50
Cs[+] (>99%)	Cs[+]	85	SOCs = 1 SOH, −1 H[+], 1 Cs[+]	−1.40
SeO_3[2-] (>99%)	SeO_3[2-]	62	SOCaSeO3[-] = 1 SOH, −1 H[+], 1 Ca[2+], 1 SeO_3[2-]	−0.15
Cl[-](>99%)		<1	– –	–

$$S - OCa^+ + Y^{z-} \underset{K_Y}{\rightarrow} S - OCaY^{(z+1)-} \quad \text{E.5}$$

In Fig. 1a, Eu and Pu sorption seems to be linear within the range of concentration analyzed. In the case of Eu, precipitation was not suggested and the solid controlling solubility, $Eu(OH)_3$, (cr) was excluded. The major aqueous species expected under experimental conditions is the neutral $Eu(OH)_3$(aq) (>99%) and the first most abundant charged species, selected for complexation reactions is $Eu(OH)_2$[+].

Similarly, the neutral $Pu(OH)_4$(aq) strongly dominates Pu speciation (>99%), even though the very small contribution of $Pu(OH)_3$[+], can be considered for surface complexation. Also in this case, the precipitation of PuO_2(am) was predicted but excluded.

Pu experiments carried out with two different portlandite solid to liquid ratios (S/L) showed different behaviour indicating that the formation of Pu colloids cannot be ruled out, when the Pu aqueous concentration exceeds $1{\cdot}10^{-11}$ M.

The electrostatic attraction between the (positively charged) portlandite and eventually formed Pu colloids (possibly negatively charged due to the high pH), could be mixed up with the adsorption mechanism.

In the case of the three additionally selected elements Cs, Ba and Cd (Fig. 2b) thermodynamic calculations indicated that the main aqueous species in the conditions generated by portlandite are Cs^+, Ba^{2+} and Cd $(OH)_3^-$ respectively. Precipitation of $Cd(OH)_2$ at an equilibrium

concentration of approximately $2.4{\cdot}10^{-7}$ M was predicted, but not observed in the experimental sorption isotherms. Cs^{+} and specially Ba^{2+}, are narrowly sorbed to portlandite. Cadmium complexation to portlandite, $Cd(OH)_3^-$ bridged by Ca (Table 5) gives rise to very high sorption values.

In the case of selenium (Fig. 2c) the main selenite species present in solution is SeO_3^{2-} In this case, when increasing the equilibrium concentration higher than 10^{-4} M, an increase of K_d values was observed, suggesting precipitation. Calculations where done both excluding and including precipitation (indicated as a vertical line in Fig. 2c), which confirms the precipitation of $Ca(SeO_3)$ (s), a Ca-selenite solid.

Chloride sorption on portlandite was under the detection limits. Positively charged surfaces as that of portlandite, should show affinity for anions like chloride but, as discussed in (Florea and Brouwers, 2012; Hirao et al., 2005), portlandite does not show high sorption affinity towards chloride; similarly (Missana et al., 2019) did not observe any adsorption on chloride in both negatively and positively charged CSH phases.

For the modelling of the adsorption isotherms for each RN, only one adsorption site and only one adsorbing species were considered, thus the logK of the specific surface reaction is the unique parameter for the fit. The logK was adjusted until the simulated K_d value corresponded to the mean experimental K_d value, observed in the linear zone. The error of the fit is therefore related to the experimental error, and the maximum estimated error on the logK for the reactions summarized in Table 5 is ± 0.2.

Table 5 presents the main species considered for surface complexation in each case, the complex formed and the obtained complexation constant, determined by fit, and the mean K_d predicted in the linear adsorption zone for each radionuclide is also indicated in Table 5.

The fits obtained for each system are superimposed to the experimental data in Fig. 2 a-c, which is quite satisfactory in all the cases.

In the case of Cs, the theoretical adsorption excluding Na competition is also plotted as (dotted line in Fig. 2b), evidencing the competitive effect of Na on Cs adsorption.

It is interesting noticing that the complexation of Ca^{2+} and Ba^{2+}, both alkaline earth metals, give rise to similar complexation constants, which is reasonable. The estimated K_d for Ca considering pH = 12.5 and [Ca] = 20 mM was 1.34 mL g^{-1}.

It is interesting that the value for Ca has been evaluated by ζ-potential measurements, whereas the value for Ba has been obtained directly by adsorption experiments being the combination of both techniques very valuable.

5. Conclusions

In this study the adsorption of different radionuclides (^{137}Cs, ^{133}Ba, ^{109}Cd, ^{152}Eu, ^{238}Pu, ^{75}Se and ^{36}Cl) was analyzed in portlandite and a double layer sorption model was applied to evaluate the experimental data. This is the first time that a surface model for portlandite is reported, which can be considered a very useful tool to quantify RN sorption processes in cementitious environments and evaluate their variations as mineral composition and chemistry evolution.

Results revealed that Ca can be considered the ion determining the potential (IDP) of portlandite but Ca consumption is not only attributed to adsorption/desorption processes at the surface, but also by further precipitation of the solid for pH > 12.5.

All the analyzed adsorption isotherms could be simulated by a simple one-site/one species double layer complexation model.

The existence of Pu colloids in the system (even within the very low range of concentrations used) cannot be ruled out and this topic is worth of further investigations.

Declaration of competing interest

The authors declare that they have no known competing financial interests or personal relationships that could have appeared to influence the work reported in this paper.

Data availability

Data will be made available on request.

Acknowledgments

This study was partially supported by the European Union's Horizon 2020 Research and Innovation Programme under Grant Agreement no. 847593 (EURAD, CORI) and by the Spanish Ministry of Science and Innovation (PID2019–106398GB-I00, ARNO Project).

References

Atkins, M., Glasser, F.P., 1992. Application of portland cement-based materials to radioactive waste immobilization. Waste Manag. Cement. Mater. Radioact. Waste Manag. 12, 105–131. https://doi.org/10.1016/0956-053X(92)90044-J.

Atkinson, A., Everitt, N.M., Guppy, R.M., 1989. Time Dependence of pH in a Cementitious Repository. Materials Research Society, United States.

Begg, J., Rodríguez, J., Perez, D., Colàs, E., Duro, L., Fuller, A.J., 2021. Track-changes and track-error document: From version 10a to version 10d (Technical report).

Borkel, C., 2016. Understanding the mobility of caesium, nickel and selenium released from waste disposal : chemical retention mechanisms of degraded cement (Ph.D. Thesis). TDX (Tesis Doctorals en Xarxa). Universitat Politècnica de Catalunya.

Chollet, M., Horgnies, M., 2011. Analyses of the surfaces of concrete by Raman and FT-IR spectroscopies: comparative study of hardened samples after demoulding and after organic post-treatment. Surf. Interface Anal. 43, 714–725. https://doi.org/10.1002/sia.3548.

Duque-Redondo, E., Yamada, K., Arbeloa, I.L., Manzano, H., 2018. Adsorption and Diffusion of Na+, Cs+ and Ca+2 Ions in C-S-H and C-A-S-H Nanopores. https://doi.org/10.26434/chemrxiv.6476510.v1.

Duque-Redondo, E., Yamada, K., Manzano, H., 2021. Cs retention and diffusion in C-S-H at different Ca/Si ratio. Cement Concr. Res. 140, 106294 https://doi.org/10.1016/j.cemconres.2020.106294.

Fernandez-Carrasco, L., Torrens-Martin, D., Morales, L.M., Martinez-Ramirez, S., 2012. Infrared Spectroscopy in the Analysis of Building and Construction Materials, Infrared Spectroscopy - Materials Science, Engineering and Technology. Intech Europe.

Florea, M.V.A., Brouwers, H.J.H., 2012. Chloride binding related to hydration products: Part I: ordinary Portland Cement. Cement Concr. Res. 42, 282–290. https://doi.org/10.1016/j.cemconres.2011.09.016.

Grambow, B., López-García, M., Olmeda, J., Grivé, M., Marty, N.C.M., Grangeon, S., Claret, F., Lange, S., Deissmann, G., Klinkenberg, M., Bosbach, D., Bucur, C., Florea, I., Dobrin, R., Isaacs, M., Read, D., Kittnerová, J., Drtinová, B., Vopálka, D., Cevirim-Papaioannou, N., Ait-Mouheb, N., Gaona, X., Altmaier, M., Nedyalkova, L., Lothenbach, B., Tits, J., Landesman, C., Rasamimanana, S., Ribet, S., 2020. Retention and diffusion of radioactive and toxic species on cementitious systems: main outcome of the CEBAMA project. Appl. Geochem. 112, 104480 https://doi.org/10.1016/j.apgeochem.2019.104480.

Hirao, H., Yamada, K., Takahashi, H., Zibara, H., 2005. Chloride binding of cement estimated by binding isotherms of hydrates. J. Adv. Concr. Technol. 3, 77–84. https://doi.org/10.3151/jact.3.77.

Horgnies, M., Chen, J.J., Bouillon, C., 2013. Overview about the Use of Fourier Transform Infrared Spectroscopy to Study Cementitious Materials. Siena, Italy, pp. 251–262. https://doi.org/10.2495/MC130221.

Kursten, B., Druyts, F., Gens, R., 2011. The Belgian Supercontainer Concept - Corrosion Issues. In*Sulphur-Assisted Corrosion in Nuclear Disposal Systems*, 1 ed. European Federation of Corrosion Publications; No. Number 59). Taylor & Francis (CRC), pp. 1–18.

Missana, T., Garcıa-Gutiérrez, M., Mingarro, M., Alonso, U., 2017. Analysis of barium retention mechanisms on calcium silicate hydrate phases. Cement Concr. Res. 93, 8–16. https://doi.org/10.1016/j.cemconres.2016.12.004.

Missana, T., García-Gutiérrez, M., Mingarro, M., Alonso, U., 2019. Selenite retention and cation coadsorption effects under alkaline conditions generated by cementitious materials: the case of C–S–H phases. ACS Omega 4, 13418–13425. https://doi.org/10.1021/acsomega.9b01637.

Missana, T., Garcıa-Gutiérrez, M., Alonso, U., Almendros-Ginestá, O., 2022. Nickel retention by calcium silicate hydrate phases: evaluation of the role of the Ca/Si ratio on adsorption and precipitation processes. Appl. Geochem. 137, 105197 https://doi.org/10.1016/j.apgeochem.2022.105197.

Ochs, M., Mallants, D., Wang, L., 2016. Radionuclide and metal sorption on cement and concrete. https://doi.org/10.1007/978-3-319-23651-3.

Östhols, E., Wanner, H., 2000. TDB-0: the NEA thermochemical database (TDB) project [WWW document]. URL Nucl. Energy Agency (NEA). accessed 7.27.22. https://www.oecd-nea.org/jcms/pl_37490/tdb-0-the-nea-thermochemical-database-tdb-project?details=true.

Payne, T., Brendler, V., Ochs, M., Baeyens, B., Brown, P.L., Davis, J., Ekberg, C., Kulik, D., Lützenkirchen, J., Missana, T., Tachi, Y., Van Loon, L., Altmann, S., 2013. Guidelines for thermodynamic sorption modelling in the context of radioactive

waste disposal. Environ. Model. Software 42, 143–156. https://doi.org/10.1016/j.envsoft.2013.01.002.

Seewald, J.S., Seyfried, W.E., 1991. Experimental determination of portlandite solubility in H2O and acetate solutions at 100–350 °C and 500 bars: constraints on calcium hydroxide and calcium acetate complex stability. Geochem. Cosmochim. Acta 55, 659–669. https://doi.org/10.1016/0016-7037(91)90331-X.

Taylor, H.F.W., 1997. Cement Chemistry. Thomas Telford.

Timmons, J., Mehdipour, I., Gao, S., Atahan, H., Neithalath, N., Bauchy, M., Garboczi, E., Srivastava, S., Sant, G., 2020. Dispersing nano- and micro-sized portlandite particulates *via* electrosteric exclusion at short screening lengths. Soft Matter 16, 3425–3435. https://doi.org/10.1039/D0SM00045K.

Van der Lee, J., de Windt, L., 1999. CHESS Tutorial and Cookbook. Ecole des Mines de Paris (Technical report No. LHM/RD/99/05).

Volchek, K., Miah, M.Y., Kuang, W., DeMaleki, Z., Tezel, F.H., 2011. Adsorption of cesium on cement mortar from aqueous solutions. J. Hazard Mater. 194, 331–337. https://doi.org/10.1016/j.jhazmat.2011.07.111.